95

NEANDC(E) 196 "L"
INDC (FR) 29/L

DIFFERENTIAL CROSS SECTION MEASUREMENTS FOR 3.4 MeV NEUTRON SCATTERING FROM ^{208}Pb, ^{232}Th, ^{235}U, ^{238}U and ^{239}Pu

G. HAOUAT, J. LACHKAR, Ch. LAGRANGE, Y. PATIN
J. SIGAUD and R.E. SHAMU

Service de Physique Nucléaire

Centre d'Etudes de Bruyères-le-Châtel

B.P. n° 561

92542 MONTROUGE CEDEX FRANCE

FEVRIER 1978

COMMISSARIAT A L'ENERGIE ATOMIQUE

FRANCE

NEANDC (E) 196 "L"
INDC (FR) 29/L

DIFFERENTIAL CROSS SECTION MEASUREMENTS FOR 3.4 MeV NEUTRON SCATTERING FROM ^{208}Pb, ^{232}Th, ^{235}U, ^{238}U and ^{239}Pu.

by

G. HAOUAT, J. LACHKAR, Ch. LAGRANGE, Y. PATIN
J. SIGAUD AND R.E. SHAMU*

Service de Physique Nucléaire
Centre d'Etudes de Bruyères-le-Châtel
B.P. N° 561
92542-MONTROUGE-CEDEX-FRANCE.

**On leave from Western Michigan University. Present Address : Western Michigan University, Kalamazoo, Michigan 49001.*

- FEB 1978 -

CONTENTS

ABSTRACT

Differential cross sections for neutron scattering from ^{208}Pb, ^{232}Th, ^{235}U, ^{238}U and ^{239}Pu have been measured at an incident energy of 3.4 MeV. The measurements were carried out using the four-angle time-of-flight neutron spectrometer of the Centre d'Etudes de Bruyères-le-Châtel. The overall energy resolution was about 28 keV. Elastic scattering cross sections are presented for ^{208}Pb, as well as separated cross sections for the elastic and inelastic scattering to the first 2^+ and 4^+ states of ^{232}Th and ^{238}U. It is the first time that the inelastic scattering to the lowest 2^+ and 4^+ states of ^{232}Th and ^{238}U is experimentally resolved from the elastic scattering at this energy. For ^{235}U and ^{239}Pu, since the experimental resolution was larger than the energy spacing of some levels, data are given for groups of levels. Large disagreements between the present data and recent evaluations are observed.

The data have been compared to calculations using a spherical optical potential for ^{208}Pb and a coupled-channel optical potential for the deformed actinide nuclei. Potential parameters have been obtained separately for each nucleus. Values of the β_2 and β_4 deformation parameters have been derived from this work for the actinide nuclei.

I - INTRODUCTION

Besides the applied interest in providing accurate data, the study of neutron scattering from actinides can bring insight into the nuclear deformation of these nuclei. The main source of information on nuclear shapes has been hitherto studies of Coulomb excitation [1] and inelastic electron scattering [2] which give the proton distribution of nuclei; there have been also studies of high-energy scattering of protons [3] and α-particules [4] which are sensitive to the distribution of protons plus neutrons in nuclei. Neutron scattering [5] has poorly contributed to our knowledge of nuclear deformations because the techniques have not had, up to this time, the requisite energy resolution that permits separation of the actinide low-lying collective state groups at incident neutron energies above $\simeq$ 2 MeV. At such high energies, the direct interaction mechanism, governed by the nuclear potential, dominates the scattering [6,7].

We have therefore developed a program to obtain information, from neutron scattering, on the deformed nuclear potential for several actinide nuclei. A first reported experiment [7] has been performed on ^{232}Th, ^{238}U and on the nearby spherical nucleus ^{208}Pb. Differential cross section measurements were taken at 2.5 MeV incident energy because calculations [8] of total cross sections for ^{238}U suggest that at this energy the deformation effects may be very large.

In the present work, scattering potential strengths are examined. It was shown recently that calculated total cross sections for Sm isotopes near 4 MeV are mainly sensitive to variations of the potential depth parameters [9]. Preliminary calculations have been done by one of us (Ch. L.) which indicate that a similar behaviour is expected to occur around 3.4 MeV for ^{238}U.

In this paper we present measurements of neutron elastic and inelastic scattering from ^{208}Pb, ^{232}Th, ^{235}U, ^{238}U and ^{239}Pu at the incident energy of 3.4 MeV, and we show a preliminary analysis of the data. In the measurements, the inelastic scattering to the lowest 2^+ and 4^+ states of ^{232}Th and ^{238}U was experimentally resolved from the elastic scattering. Since the low-lying level spacing in ^{235}U and ^{239}Pu (fig.1) is substantially smaller than the energy resolution of our experimental system, only composite cross sections for some groups of states were obtained for these nuclei.

II - EXPERIMENTAL SYSTEMS AND PROCEDURES

Differential cross section measurements were performed using the four detector neutron time-of-flight spectrometer of the Centre d'Etudes de Bruyères-le-Châtel tandem accelerator laboratory. The experimental arrangement is extensively described elsewhere [7,10] and therefore only a brief description is given here.

1. *Experimental system*

Incident neutrons of 3.4 MeV energy were produced using the $^{7}Li(p,n_{o})^{7}Be$ reaction. The proton beam from the accelerator was pulsed and bunched into 0.7 ns bursts (FWHM) with a repetition rate of 2.5 MHz. The average current was typically 2 μA. The beam was incident on a thin target which consisted of 99.8 % pure ^{7}Li evaporated on a 2-cm-diameter by 1-mm- thick tantalum disc. The energy spread of the incident neutrons, due to lithium thickness, was about 10 keV.

The neutrons were incident on cylindrical samples located at 0 deg with respect to the proton beam axis and at 10.3 cm from the target. The ^{208}Pb, ^{232}Th, ^{235}U, ^{238}U and ^{239}Pu samples were 1.5-cm-diameter solid metal cylinders having the same number of atoms (0.294 mole). The isotopic enrichment of the actinides was greater than 99.5 % ; for ^{208}Pb it was 86.5 %. The ^{239}Pu sample was placed in a nickel can which was sealed and put in a polyethylene container. The scattered neutrons were detected by an array of four recoil proton detectors placed at 20 deg intervals. Each detector was composed of a 10-cm-diameter by 2.5-cm-thick NE 213 liquid scintillator optically coupled to an XP-1040 photomultiplier tube. Each detector was housed in a heavy shield of lead and paraffin loaded with lithium carbonate and borax. Four 1-m-long shadow bars made of polyethylene and lead intercepted neutrons from the source in the detector direction. Intermediate 1.5-and 0.5-m-long collimators of paraffin, loaded with $Li\,CO_3$ and borax, were placed between the detector shielding and the shadow bars ; they greatly reduced time independent background in the scattered neutron spectra. The flight path from the sample to each detector was 10 m. For this distance the energy spreads and time spreads of the experiment, including incident neutron energy spread, sample size, scintillator thickness and electronic time resolution, were such that the overall energy resolution of the measurements was $\leqslant$ 28 keV. A time-of-flight spectrum for the ^{238}U sample is shown in fig. 2 to illustrate the experimental resolution.

Data were collected using standard time-of-flight techniques with n-γ pulse shape discrimination to reject γ-ray induced events in scintillators. A two-parameter data acquisition system recorded flight time and recoil proton pulse height for each detected event, so that the detector pulse height bias could be adjusted in off-line data analysis to minimize uncertainties in the yields extracted from the time-of-flight spectra.

The primary neutron flux was monitored by counting, with a Ge(Li) diode, the 431-and 478-keV γ-rays, produced by proton induced reactions in ^{7}Li. An auxiliary neutron detector was used also as a monitor, in the time-of-flight mode. The γ-ray and neutron monitoring systems were consistent with each other to within 1 % throughout the course of the measurements.

The energy dependence of the detector efficiency was determined between 3.0 and 3.4 MeV relative to the efficiency at 3.4 MeV : we compared measurements of the neutron yields from the ^{7}Li(p,n)^{7}Be reaction for the ground and first excited states of Be with the known cross sections for that reaction [11]. The absolute efficiency was not needed : we removed the sample and brought the detector to 0 deg with respect to the proton beam axis and at 10 m from the neutron source in order to measure the incident neutron flux. Hence the incident and scattered neutron fluxes were measured with the same detector.

2. *Measurements and Corrections*

Measurements were completed over the angular range from 20 to 160 deg at 19 angles. Sample-in and sample-out runs were taken. In addition, empty container runs were taken in order to subtract nickel and polyethylene contributions to the ^{239}Pu neutron spectra. For each scattered neutron spectrum, background subtraction was achieved. Yields were obtained for isolated peaks in the spectra both by direct summation of counts and also by fitting gaussian forms to the peaks. For ^{232}Th and ^{238}U, the ground state (g.s) and first excited state neutron groups were so close to each other that yields were obtained only by fitting procedures. For ^{235}U and ^{239}Pu, the energy spacing of some levels (fig.1) was substantially smaller than the experimental resolution so that separation of all the state groups could not be done. Therefore yields were extracted for groups of levels. A time-of-flight spectrum is presented in fig. 3 for ^{235}U and in fig.4 for ^{239}Pu showing the scattered neutron groups and the corresponding levels.

The net yields were corrected for anisotropy effects in the incident neutron flux and finite size effects in the sample. These latter corrections included those for neutron flux attenuation by the sample, multiple scattering and geometrical effects; the corrections were made using the analytical method described by Kinney [12].

Normalization uncertainties assigned to the data were small since the incident and scattered neutron fluxes were measured with the same detector. Uncertainties in the measurements arose from counting statistics and background subtraction, monitor counting dispersion, detector efficiency and sample corrections. These contributions, listed in table 1, were added quadratically to give the experimental uncertainties.

III - RESULTS AND INTERPRETATION

1. *Results*

We present here differential scattering cross sections obtained at 3.4 MeV incident neutron energy for ^{208}Pb, ^{232}Th, ^{235}U, ^{238}U and ^{239}Pu. For ^{208}Pb, only elastic scattering cross sections were determined since the minimum available energy threshold of the detectors was 0.9 MeV and could not hence permit detection of neutrons scattered from the first 3^- (2.615 MeV) and 5^- (3.198 MeV) states. The data for ^{208}Pb are presented in fig. 5. The curves in this and subsequent figures up to fig. 9, are the results of calculations to be described in Sec.III.2. Cross sections were obtained for the elastic (0^+) and inelastic scattering to the first 2^+ and 4^+ states of ^{232}Th (fig.6) and ^{238}U (fig.7). Because the experimental resolution is larger than the energy spacing of some levels of ^{235}U, cross sections were determined for the two groups of levels : ($7/2^-$ (g.s), $1/2^+$, $3/2^+$) and ($9/2^-$, $5/2^+$), they are displayed in fig.8 ; also given in this figure are the cross sections for the $11/2^-$ state. However the states of the rotational band built on the $1/2^+$ (75 eV) particle level seem to be very weakly excited, since the neutron group corresponding to the $7/2^+$ (84 keV) state of this band is not conspicuous in the time-of-flight spectra (see fig.3). Moreover scattered neutrons corresponding to the $3/2^+$ (13 keV) and $5/2^+$ (52 keV) do not seem to broaden the elastic ($7/2^-$) and inelastic ($9/2^-$) neutron peaks respectively (fig. 3). For ^{239}Pu also, cross sections were obtained for the three groups of levels : ($1/2^+$ (g.s), $3/2^+$), ($5/2^+$, $7/2^+$) and

$(9/2^+, 11/2^+)$, they are displayed in fig. 9. Data could not be extracted for the $(9/2^+, 11/2^+)$ group below 60 deg because the corresponding neutron group could not be separated from the contaminant peak produced by scattering from carbon in the sample container. The differential cross sections and their uncertainties are quoted in tables 2 to 14. Also given in these tables are the coefficients of a least-squares fit of the data to a Legendre polynomial expansion. The method for deriving these coefficients and their uncertainties has been described elsewhere [13]. The data and their uncertainties, as obtained prior to sample corrections with the formula of ref. 7 are also quoted in tables 2 to 14.

One notes that the elastic scattering angular distribution of ^{208}Pb (fig.5) is smoother in shape than the ^{232}Th and ^{238}U elastic distributions (figs 6-7). On the other hand, comparison between ^{232}Th (fig.6) and ^{238}U (fig.7) shows that the differential cross sections are almost identical for the two isotopes, with barely discernable differences at large angles for the elastic (0^+) scattering, and at forward angles for the inelastic scattering to the 4^+ state. This implies that these nuclei have a similar behaviour with regards to neutron scattering. The angular distributions of ^{235}U (fig.8) and ^{239}Pu (fig.9) are rather similar in shape to those of the even-even actinides, but direct comparison cannot be made since the cross sections presented here include contributions of several states.

The present elastic scattering differential cross section data are compared, in fig. 10, with the latest ENDF/B IV and ENDL 76 evaluations. In this figure, the solid lines represent the results of calculations to be described below ; the dotted and dashed curves are the angular distributions obtained from the ENDF/B IV and ENDL 76 files, respectively. For the actinide nuclei large disagreements between experimental and evaluated data are observed mainly at angles beyond $\simeq$ 45 deg : the two minima around 55 deg and 120 deg in the measured angular distributions are not reproduced by the evaluations. This may be explained by the fact that these evaluations are based on poor resolution measurements [14-16] which include contributions from many unresolved levels. For ^{208}Pb, discrepancies remain even at forward angles. The disagreement between evaluated and measured inelastic scattering cross sections for the actinide nuclei is worse. All the evaluated inelastic angular distributions are considered as isotropic in both files, and the angle-integrated cross sections are much smaller than the experimental data except for the ENDL 76 values for ^{238}U (see table 15)

2. *Interpretation*

A preliminary approach to the analysis of the data has been attempted. The elastic scattering differential cross sections of ^{208}Pb were calculated using the conventional spherical model to take into account the direct interaction process, and the Wolfenstein-Hauser-Feshbach formalism [17] to estimate the compound elastic cross sections. For the permanently deformed actinide nuclei, the analysis was carried out using the coupled-channel optical model [18]. The compound nucleus contribution to the scattering from the actinides was found to be negligible for the elastic and inelastic scattering at 3.4 MeV ; it was thus ignored.

In addition to the data of this experiment, the analysis included previous results on ^{208}Pb, ^{232}Th and ^{238}U from this laboratory [7], and also neutron data from a few keV to 15 MeV [6,19]. The optical potential was assumed to have the following form :

$$U = - V_R \, f(r,a_R,R_R) + i \, W_D . 4 . a_D \frac{d}{dr} f\,(r,a_D,R_D) + \left(\frac{\hbar}{m_\pi c}\right)^2 V_{SO} . \vec{\ell} . \vec{\sigma} . \frac{1}{r} \frac{d}{dr} f\,(r,a_{SO},R_{SO}) \qquad (1)$$

the form factor f is $f(r,a,R) = \left[1 + \exp\,(r - R)/a\right]^{-1}$. For the spherical optical model analysis the radii are expressed as $R = R^{\circ} A\ 1/3$. For the deformed optical model analysis the radii were taken as :

$$R = R^{\circ} A^{1/3} \left[1 + \beta_2 Y_{20}(\theta) + \beta_4 Y_{40}(\theta)\right] \qquad (2)$$

for the deformable terms V_R and W_D. The spin-orbit potential V_{SO} was not deformed and we had $R_{SO} = R^{o}_{SO} A^{1/3}$. The β_2 and β_4 parameters of formula 2 are, respectively, the quadrupole and hexadecapole deformation parameters of the nucleus.

Coupled-channel calculations were performed using a modified version [20] of Tamura's code [21] JUPITOR-1. The geometric parameters R^{o}_{R}, R^{o}_{D}, R^{o}_{SO}, a_R, a_D and a_{SO} were taken the same for the five nuclei (see table 16). The other potential parameters were adjusted separately for each nucleus. The potential depths were first estimated using the parametrization method proposed by Lagrange [22] and then adjusted to fit the present data (table 16). The deformation parameters of the actinide nuclei were accurately determined from the present and previous [7] elastic and inelastic scattering data.

It is shown in fig.5, for ^{208}Pb, that the agreement between experimental and calculated elastic cross sections is very good at forward angles. Some minor differences remain at large angles ; these differences may be attributed to an overestimate of the compound elastic cross sections, or to effects of resonances, observed in the total cross section near 3.4 MeV by Foster and Glasgow [23], which were not taken into account in the present analysis. One notes that the compound nucleus process is responsible for the smoother shape of the elastic angular distribution of ^{208}Pb (fig.5) compared to that of the elastic distribution of ^{232}Th (fig.6) and ^{238}U (fig.7).

Calculations were made for ^{232}Th and ^{238}U assuming a coupling basis 0^+, 2^+, 4^+. Figs.6 and 7 show that a good overall agreement between calculations and data was obtained when using the same values of potential and deformation parameters as in ref.7, the only difference being the very slight change (0.2 MeV) in the real potential depth of ^{232}Th (see table 16). Nevertheless, the structures in the 2^+ experimental cross sections for both ^{232}Th and ^{238}U are not well reproduced by calculation. This failure will be discussed below.

Calculations of the ^{235}U cross sections were carried out assuming the strong coupling of the $7/2^-$, $9/2^-$ and $11/2^-$ states of the ground-state rotational band. The good agreement between experimental and calculated cross sections (fig.8) would suggest that the above assumption is adequate and that the excitation of the low-lying states of the rotational band built on the $1/2^+$ (75 eV) particle level is relatively weak.

Cross sections for the first six states of the ground-state rotational band of ^{239}Pu were computed using the coupled-channel adiabatic approximation [18]. Calculated values (dashed curves) are presented in fig.9 along with the experimental data for the ($1/2^+$, $3/2^+$), ($5/2^+$, $7/2^+$) and ($9/2^+$, $11/2^+$) groups of states. Satisfactory agreement is obtained for the ($1/2^+$, $3/2^+$) group, but for the two other groups calculations are substantially smaller than the data. We turned, then, to calculations taking into account explicitly the strong coupling of the $1/2^+$, $3/2^+$, $5/2^+$, $7/2^+$, $9/2^+$ states; these last calculations displayed as solid lines in fig.9, are in better overall agreement with the data.

Values of the deformation parameters extracted from the present analysis are given in table 17 for ^{232}Th, ^{238}U, ^{235}U and ^{239}Pu, with an estimated accuracy of 5 % for β_2 values and 10 % for β_4 values. Comparison of the β_2 values implies that the static deformation is rather larger for the two even-odd nuclei than for the two even-even ones.

The real and imaginary potential depths, derived here for the actinide nuclei, have very similar values (table 16). These values are not definitive and a further analysis should precise the isospin dependence of the potentials. On the other hand, the imaginary term for ^{208}Pb is much smaller than that for the actinide nuclei. This behaviour may be ascribed to the nuclear shell closure effects on neutron optical model absorption [24,25].

As noticed above, the structure of the calculated curve of inelastic scattering to the 2^+ state of ^{232}Th and ^{238}U is less pronounced than that of the data (figs. 6-7). The same failure appears in the ($5/2^+$, $7/2^+$) angular distributions of ^{239}Pu (fig.9). Previous analyses of Sm and Nd inelastic data show a similar deficiency [26-28]. It is possible that the observed structure could be reproduced by coupling in several additional channels. Another possibility is that the surface coupling term of the collective model may not be realistic [29]. Future analysis effort will be to examine these assumptions.

IV - SUMMARY

Differential cross sections for neutron scattering by ^{208}Pb, ^{232}Th, ^{235}U, ^{238}U and ^{239}Pu have been measured at 3.4 MeV with an energy resolution of about 28 keV. Angular distributions were obtained for elastic scattering by ^{208}Pb, ^{232}Th and ^{238}U and for inelastic scattering to the first 2^+ and 4^+ states of ^{232}Th and ^{238}U. It is the first time that the inelastic scattering to the first 2^+ and 4^+ states of ^{232}Th and ^{238}U is experimentally resolved from the elastic scattering at 3.4 MeV. Cross sections were also obtained for the following groups of states : ($1/2^+$ (g.s), $3/2^+$), ($5/2^+$, $7/2^+$), ($9/2^+$, $11/2^+$) for ^{239}Pu and ($7/2^-$ (g.s), $1/2^+$, $3/2^+$), ($9/2^-$, $5/2^+$) and $11/2^-$ for ^{235}U. For this last nucleus, it seems that the excitation of the collective states of the rotational band built on the $1/2^+$ (75 eV) particle level is relatively weak. Significant discrepancies between the present data and the ENDF/B IV and ENDL 76 evaluations have been shown.

The data have been compared to calculations in which a spherical optical potential was used for ^{208}Pb and a deformed optical potential for the actinide nuclei. In the analysis presented here, the derived values of the actinide potential parameters are very similar. The smaller value of the imaginary potential of ^{208}Pb may be attributable to shell closure effects. Values of the β_2 and β_4 deformation parameters obtained for the actinide nuclei show that the ^{235}U and ^{239}Pu nuclei seem to be more deformed than the ^{232}Th and ^{238} nuclei.

REFERENCES -

[1] - C.E. BEMIS, F.K. Mc GOWAN, J.L.C. FORD, W.T. MILNER, R.H. STELSON and R.L. ROBINSON, *Phys. Rev.* C8 *(1973) 1466.*

[2] - T. COOPER, W. BERTOZZI, J. HEISENBERG, S. KOWALSKI, W. TURCHINETZ, C. WILLIAMSON, L. CARDMAN, S. FIVOZINSKY, J. LIGHTBODY Jr. and S. PENNER, *Phys. Rev.* C13 *(1976) 1083.*

[3] - C.H. KING, G.H. CRAWLEY, J.A. NOLEN Jr. and J. FINK, *Proceeding of the International Conference on Nuclear Structure TOKYO (1977) 504.*

[4] - P. DAVID, J. DEBRUS, H. ESSEN, F. LÜBKE, H. MOMMSEN, R. SCHOENMACKERS, W. SOYEZ, H.V. von GERAMB and E.F. HEFTER, *Z. Physik* A278 *281.*

- D.L. HENDRIE, B.G. HARVEY, J.R. MERIWETHER, J. MAHONEY, J.C. FAIVRE and D.G. KOVAR, *Phys. Rev. Lett.* 30 *(1973) 571.*

[5] - P. GUENTHER and A. SMITH, *in Nuclear Cross Sections and Technology, etited by R.A. SCHRACK and C.D. BOWMAN, National Bureau of Standards Special Publication n° 425 (1975) 862.*

[6] - Ch. LAGRANGE, *NEANDC Report JAERI-M-5984 (1975) 58.*

[7] - G. HAOUAT, J. SIGAUD, J. LACHKAR, Ch. LAGRANGE, B. DUCHEMIN and Y. PATIN, *Report NEANDC (E) 180 "L", INDC (FR) 13/L (1977).*

[8] - Ch. LAGRANGE, *J. Phys. Lett.* 35 *(1974) 111.*

[9] - R.E. SHAMU, Ch. LAGRANGE, E.M. BERNSTEIN, J.J. RAMIREZ, T. TAMURA and C.Y. WONG, *Phys.Lett.* 61B *(1976) 29.*

[10] - J. LACHKAR, M.T. Mc ELLISTREM, G. HAOUAT, Y. PATIN, J. SIGAUD and F. COÇU, *Phys. Rev.* C14 *(1976) 933.*

[11] - H. LISKIEN and A. PAULSEN, *Atomic Data and Nuclear Data Tables* *15 (1975) 57.*

[12] - W.E. KINNEY, *Nucl. Inst. and Meth. 83 (1970) 15.*

[13] - G. HAOUAT, J. LACHKAR, J. SIGAUD, Y. PATIN and F. COÇU, *Nucl. Sci. and Eng. 65 (1978) 331 ; also* G. HAOUAT, J. LACHKAR, J. SIGAUD, Y. PATIN and F. COÇU, *CEA Report CEAR-R-4641 (1975).*

[14] - R. BATCHELOR, W.B. GILBOY and J.H. TOYLE, *Nucl. Phys. 65 (1965) 236.*

[15] - M. WALT and J.R. BEYSTER, *Los Alamos report n° 2061 (1956).*

- H.H. KNITTER, M. COPPOLA, N. AHMED and B. JAY, *Z. Physik 244 (1971) 358.*

[16] - R. BATCHELOR and K. WYLD, *AWRE report 055/69 (1969).*

- H.H. KNITTER, M.M. ISLAM and H. COPPOLA, *Z. Physik 257 (1972) 108.*

[17] - L. WOLFENSTEIN, *Phys. Rev. 82 (1951) 690.*
- W. HAUSER and H. FESHBACH, *Phys. Rev. 87 (1952) 366.*
- E. SHELDON and D.M. VAN PATTER, *Rev. Mod. Phys. 38 (1966) 143.*

[18] - T. TAMURA, *Rev. Mod. Phys. 37 (1965) 679.*

[19] - J. JARY, Ch. LAGRANGE and P. THOMET, *INDC (FR) 9/L, NEANDC (E) 174 "L" (1976).*

[20] - Ch. LAGRANGE and N. MONDON, *Internal Report, Centre d'Etudes de LIMEIL, France (1973) (unpublished).*

[21] - T. TAMURA, *ORNL-4152 (1967) (unpublished).*

[22] - J.P. DELAROCHE, Ch. LAGRANGE and J. SALVY, *Nuclear Theory in Neutron Nuclear Data Evaluation, IAEA-190 Vol II (1976) 251.*

[23] - D.J. FOSTER and D.W. GALSGOW, *Phys. Rev. C3 (1971) 576.*

[24] - A.M. LANE, J.E. LYNN, E. MELKONIAN and E.R. RAE, *Phys. Rev. Lett.* *2 (1959) 424.*

[25] - W.G. VONACH, A.B. SMITH and P.A. MOLDAUER, *Phys. Lett. 11 (1964) 331.*

[26] - M.T. Mc ELLISTREM, R.E. SHAMU, J. LACHKAR, G. HAOUAT, Ch. LAGRANGE, Y. PATIN, J. SIGAUD and F. COÇU, *Phys. Rev. C15 (1977) 927.*

[27] - G. HAOUAT, J. LACHKAR, Ch. LAGRANGE, M.T. Mc ELLISTREM, Y. PATIN, R.E. SHAMU and J. SIGAUD, *Bull. Am. Phys. Soc. 20 (1975) 1196.*

[28] - D.F. COOPE, S.N. TRIPATHI, M.C. SCHELL, J.L. WEIL and M.T. Mc ELLISTREM, *Phys. Rev. C16 (1977) 2223.*

[29] - G.R. SATCHLER, *Phys. Lett. 39B (1972) 495.*

TABLE 1

Uncertainty estimates for cross section measurements

- Counting statistics in the peak and background subtraction	1 - 35 %
- Dispersion of monitor indications	< 1 %
- Detector efficiency	1 - 2 %
- Sample corrections	1 - 3 %

TABLE 2 : *SCATTERING OF 3.400 ± 0.*
LEVEL : 0.0 MeV (0^+)

PRIOR TO SAMPLE CORRECTIONS

θ_{LAB}(deg)	$d\sigma/d\Omega_{LAB}$(mb/sr)	Error (mb/sr)
20.0	4129.0	280.8
30.0	2014.0	120.8
40.0	818.0	58.1
45.0	482.2	33.8
50.0	235.8	19.1
60.0	151.2	13.0
65.0	202.3	15.0
70.0	231.2	19.2
80.0	251.3	19.9
85.0	251.2	18.3
90.0	228.5	18.7
100.0	166.8	14.7
105.0	154.1	11.7
110.0	124.9	10.1
120.0	126.2	11.7
130.0	144.2	11.5
140.0	155.4	13.8
150.0	204.3	15.5
160.0	227.6	18.0

.010 MEV NEUTRONS FROM ^{208}Pb

AFTER SAMPLE CORRECTIONS

θ_{CM} (deg)	$d\sigma/d\Omega_{CM}$(mb/sr)	Error (mb/sr)
20.1	5388.8	366.4
30.1	2487.0	149.2
40.2	902.3	64.1
45.2	476.1	33.3
50.2	175.5	14.2
60.2	112.4	9.7
65.2	198.2	14.7
70.3	246.8	20.5
80.3	279.0	22.0
85.3	279.0	20.4
90.3	248.1	20.3
100.3	167.1	14.7
105.3	152.3	11.7
110.3	115.5	9.4
120.2	121.3	11.3
130.2	146.3	11.3
140.2	158.3	14.1
150.1	220.2	16.7
160.1	247.2	19.5

LEGENDRE POLYNOMIAL COEFFICIENTS

L	A_L (mb/sr)	Error (%)
0	607.58	5.6
1	1159.76	8.1
2	1592.30	8.7
3	1620.43	9.7
4	1565.33	9.9
5	1073.90	12.1
6	503.96	21.3
7	135.96	57.2
8	20.42	280.5

TABLE 3 : *SCATTERING OF 3.400 ± 0.*
LEVEL : 0.0 MeV (0^+)

PRIOR TO SAMPLE CORRECTIONS

θ_{LAB}(deg)	$d\sigma/d\Omega_{LAB}$(mb/sr)	Error (mb/sr)
20.0	2507.0	255.7
30.0	1476.0	94.5
40.0	301.5	33.5
45.0	166.3	11.6
50.0	43.4	5.9
60.0	39.7	6.0
65.0	74.0	6.3
80.0	91.4	11.8
85.0	89.1	7.3
90.0	80.2	9.2
100.0	40.8	6.7
105.0	26.8	3.4
110.0	14.5	3.1
120.0	8.5	2.6
130.0	7.2	2.3
140.0	9.7	3.2
150.0	15.7	3.2
160.0	37.5	6.5

.010 MEV NEUTRONS FROM ^{232}Th

AFTER SAMPLE CORRECTIONS

θ_{CM} (deg)	$d\sigma/d\Omega_{CM}$(mb/sr)	Error (mb/sr)
20.1	3309.7	337.6
30.1	1907.4	122.1
40.2	333.7	37.0
45.2	163.9	11.5
50.2	17.9	2.4
60.2	32.6	4.9
65.2	84.3	7.2
80.2	110.2	14.2
85.2	106.9	8.8
90.2	95.3	11.0
100.2	44.9	7.4
105.2	27.8	3.5
110.2	13.0	2.8
120.2	7.2	2.2
130.2	6.9	2.2
140.2	10.1	3.3
150.1	17.5	3.6
160.1	47.1	8.1

LEGENDRE POLYNOMIAL COEFFICIENTS

L	A_L (mb/sr)	Error (%)
0	335.76	12.1
1	819.51	13.8
2	1087.03	15.1
3	1172.21	15.7
4	1151.30	15.2
5	854.62	17.0
6	484.23	22.6
7	179.63	38.7
8	49.92	74.8

TABLE 4 : *SCATTERING OF 3.400 ± 0.*
LEVEL : 0.050 MeV (2^+)

PRIOR TO SAMPLE CORRECTIONS

θ_{LAB}(deg)	$d\sigma/d\Omega_{LAB}$(mb/sr)	Error (mb/sr)
40.0	72.9	9.9
45.0	69.9	6.2
50.0	33.6	5.6
60.0	27.8	4.9
65.0	34.4	3.9
80.0	44.0	6.7
85.0	43.3	4.5
90.0	39.7	5.9
100.0	20.5	4.6
105.0	13.0	2.2
110.0	14.0	3.1
120.0	9.1	3.1
130.0	20.9	4.0
140.0	25.4	5.2
150.0	27.1	4.4
160.0	18.4	4.3

.010 MEV NEUTRONS FROM ^{232}Th

AFTER SAMPLE CORRECTIONS

θ_{CM} (deg)	$d\sigma/d\Omega_{CM}$(mb/sr)	Error (mb/sr)
40.2	88.0	12.0
45.2	84.3	7.4
50.2	36.1	6.1
60.2	29.4	5.2
65.2	38.8	4.3
80.2	53.4	8.2
85.2	52.6	5.5
90.2	47.9	7.1
100.2	22.3	5.0
105.2	12.6	2.2
110.2	13.9	3.1
120.2	8.7	2.9
130.2	25.0	4.8
140.2	30.6	6.3
150.1	32.1	5.2
160.1	20.1	4.7

LEGENDRE POLYNOMIAL COEFFICIENTS

L	A_L (mb/sr)	Error (%)
0	44.74	13.1
1	45.83	30.7
2	36.39	52.6
3	19.43	106.0
4	24.22	81.1
5	16.62	102.0
6	- 37.27	41.4
7	- 24.29	50.2

TABLE 5 : *SCATTERING OF 3.400 ± 0.010 MEV NEUTRONS FROM ^{232}Th*
LEVEL 0.162 MeV (4^+)

PRIOR TO SAMPLE CORRECTIONS			AFTER SAMPLE CORRECTIONS		
θ_{LAB}(deg)	$d\sigma/d\Omega_{LAB}$(mb/sr)	Error (mb/sr)	θ_{CM} (deg)	$d\sigma/d\Omega_{CM}$(mb/sr)	Error (mb/sr)
40.0	30.3	5.3	40.2	37.0	6.4
45.0	22.5	3.0	45.2	26.8	3.6
50.0	21.0	4.4	50.2	24.9	5.2
60.0	16.8	3.6	60.2	19.7	4.2
65.0	15.3	2.4	65.2	17.9	2.8
80.0	11.6	2.8	80.2	13.5	3.3
85.0	10.7	2.0	85.3	12.4	2.4
90.0	9.4	2.8	90.3	10.8	3.2
100.0	6.1	2.5	100.2	6.7	2.7
105.0	7.8	1.7	105.2	9.0	2.0
110.0	6.5	2.0	110.2	7.4	2.3
120.0	5.8	2.4	120.2	6.6	2.8
130.0	4.2	1.7	130.2	4.6	1.9
140.0	3.2	1.9	140.2	3.4	2.0
150.0	2.3	1.2	150.1	2.3	1.2

LEGENDRE POLYNOMIAL COEFFICIENTS

L	A_L (mb/sr)	Error (%)
0	14.53	6.3
1	18.16	11.3
2	8.28	32.9
3	4.34	68.7
4	1.42	138.0

TABLE 6 : *SCATTERING OF 3.400 ± 0.010 MEV NEUTRONS FROM ^{238}U*
LEVEL : 0.0 MeV (0^+)

PRIOR TO SAMPLE CORRECTIONS

θ_{LAB} (deg)	$d\sigma/d\Omega_{LAB}$ (mb/sr)	Error (mb/sr)
20.0	1892.0	115.4
30.0	1052.0	65.2
40.0	251.0	19.3
45.0	135.4	11.0
50.0	47.6	5.8
60.0	37.6	5.5
65.0	63.9	6.2
80.0	81.8	8.8
85.0	76.7	7.1
90.0	64.9	6.5
100.0	28.4	3.6
105.0	23.4	3.2
110.0	11.6	2.1
120.0	4.6	1.3
130.0	5.9	1.5
140.0	11.6	2.1
150.0	18.7	2.8
160.0	25.4	3.3

AFTER SAMPLE CORRECTIONS

θ_{CM} (deg)	$d\sigma/d\Omega_{CM}$ (mb/sr)	Error (mb/sr)
20.1	2867.2	174.9
30.1	1540.5	95.5
40.2	310.0	23.9
45.2	144.7	11.7
50.2	27.7	3.4
60.2	37.1	5.4
65.2	84.6	8.2
80.2	113.9	12.2
85.2	105.6	9.8
90.2	87.4	8.7
100.2	33.4	4.2
105.2	27.0	3.6
110.2	10.7	1.9
120.2	2.5	0.7
130.2	5.8	1.5
140.2	14.5	2.7
150.1	24.6	3.7
160.1	33.9	4.4

LEGENDRE POLYNOMIAL COEFFICIENTS

L	A_L (mb/sr)	Error (%)
0	289.89	9.2
1	701.52	10.6
2	922.40	11.7
3	992.69	12.1
4	981.33	11.4
5	740.68	12.6
6	409.15	17.9
7	157.46	30.0
8	38.23	63.6

^{238}

<u>TABLE 7</u> : *SCATTERING OF 3.400 ± 0.010 MEV NEUTRONS FROM ^{238}U*
LEVEL : 0.045 MeV (2^+)

PRIOR TO SAMPLE CORRECTIONS			AFTER SAMPLE CORRECTIONS		
θ_{LAB}(deg)	$d\sigma/d\Omega_{LAB}$(mb/sr)	Error (mb/sr)	θ_{CM} (deg)	$d\sigma/d\Omega_{CM}$(mb/sr)	Error (mb/sr)
40.0	60.3	7.1	40.2	82.2	9.7
45.0	47.1	5.0	45.2	61.9	6.6
50.0	36.5	5.0	50.2	45.9	6.2
60.0	29.5	4.7	60.2	36.5	5.9
65.0	33.7	3.9	65.2	43.9	5.1
80.0	37.6	5.4	80.2	51.3	7.4
85.0	37.0	4.3	85.2	50.3	5.8
90.0	38.7	4.3	90.2	52.9	5.8
100.0	24.3	3.2	100.2	30.7	4.1
105.0	17.4	2.6	105.2	20.4	3.1
110.0	15.1	2.4	110.2	17.2	2.8
120.0	10.0	2.0	120.2	10.4	2.1
130.0	25.3	3.4	130.2	34.6	4.6
140.0	31.0	3.8	140.2	43.0	5.2
150.0	21.9	3.0	150.1	28.4	3.9
160.0	16.5	2.6	160.1	19.9	3.1

LEGENDRE POLYNOMIAL COEFFICIENTS

L	A_L (mb/sr)	Error (%)
0	45.87	12.3
1	41.19	33.3
2	28.69	66.7
3	17.37	120.5
4	25.63	78.1
5	21.06	82.8
6	- 29.35	52.3
7	- 16.30	69.8

TABLE 8 : SCATTERING OF 3.400 ± 0.010 MEV NEUTRONS FROM ^{238}U
LEVEL : 0.148 MeV (4^+)

PRIOR TO SAMPLE CORRECTIONS			AFTER SAMPLE CORRECTIONS		
θ_{LAB}(deg)	$d\sigma/d\Omega_{LAB}$(mb/sr)	Error (mb/sr)	θ_{CM} (deg)	$d\sigma/d\Omega_{CM}$(mb/sr)	Error (mb/sr)
40.0	16.1	3.3	40.2	21.9	4.5
45.0	16.1	2.5	45.2	22.2	3.5
50.0	11.9	2.7	50.2	15.8	3.5
60.0	9.4	2.6	60.2	12.2	3.3
65.0	7.8	1.7	65.2	9.9	2.1
80.0	7.0	2.2	80.2	9.0	2.8
85.0	7.5	1.6	85.2	9.9	2.2
90.0	7.6	1.9	90.2	10.1	2.6
105.0	7.3	1.6	105.2	9.7	2.2
110.0	6.4	1.5	110.2	8.4	2.0
120.0	5.3	1.4	120.2	6.8	1.8
130.0	5.1	1.3	130.2	6.6	1.7
140.0	3.9	1.2	140.2	4.8	1.5
150.0	3.2	1.1	150.1	3.9	1.3
160.0	2.6	0.9	160.1	3.1	1.1

LEGENDRE POLYNOMIAL COEFFICIENTS

L	A_L (mb/sr)	Error (%)
0	11.72	6.6
1	11.43	14.6
2	6.89	32.5
3	7.53	32.6
4	2.64	64.0

TABLE 9 : SCATTERING OF 3.400 ± 0.010 MEV NEUTRONS FROM ^{235}U

LEVELS : 0.0 MeV $(7/2^-)$
0.000075 MeV $(1/2^+)$
0.013 MeV $(3/2^+)$

PRIOR TO SAMPLE CORRECTIONS			AFTER SAMPLE CORRECTIONS		
θ_{LAB}(deg)	$d\sigma/d\Omega_{LAB}$(mb/sr)	Error (mb/sr)	θ_{CM} (deg)	$d\sigma/d\Omega_{CM}$(mb/sr)	Error (mb/sr)
20.0	2196.0	224.0	20.1	3315.2	338.1
30.0	1087.0	71.7	30.1	1566.1	103.4
40.0	315.8	34.7	40.2	389.3	42.8
45.0	145.3	11.2	45.2	145.5	11.2
50.0	57.9	5.9	50.2	31.7	3.2
60.0	47.0	7.0	60.2	45.4	6.8
65.0	70.1	6.1	65.2	89.1	7.8
70.0	100.3	8.9	70.2	139.9	12.5
80.0	91.2	11.6	80.2	124.6	15.8
85.0	92.5	7.7	85.2	126.2	10.5
90.0	67.8	6.8	90.2	88.1	8.8
100.0	32.1	4.8	100.2	35.9	5.3
105.0	28.6	3.2	105.2	32.2	3.6
110.0	14.8	2.5	110.2	13.2	2.2
120.0	9.6	2.5	120.2	8.2	2.1
130.0	10.9	2.2	130.2	11.6	2.4
140.0	18.7	3.5	140.2	23.3	4.4
150.0	24.8	3.4	150.1	31.3	4.3
160.0	35.9	5.0	160.1	47.2	6.6

LEGENDRE POLYNOMIAL COEFFICIENTS

L	A_L (mb/sr)	Error (%)
0	317.33	7.7
1	752.61	9.0
2	989.84	10.0
3	1056.58	10.4
4	1047.60	9.8
5	785.42	10.8
6	427.07	15.2
7	153.21	27.7
8	35.78	64.3

TABLE 10 : SCATTERING OF 3.400 ± 0.010 MEV NEUTRONS FROM ^{235}U
LEVELS : 0.046 MeV (9/2−)
0.052 MeV (5/2+)

PRIOR TO SAMPLE CORRECTIONS			AFTER SAMPLE CORRECTIONS		
θ_{LAB}(deg)	$d\sigma/d\Omega_{LAB}$(mb/sr)	Error (mb/sr)	θ_{CM} (deg)	$d\sigma/d\Omega_{CM}$(mb/sr)	Error (mb/sr)
40.0	42.0	6.5	40.2	55.5	8.5
45.0	32.1	3.5	45.2	40.8	4.4
50.0	19.7	3.0	50.2	22.3	3.4
60.0	17.2	3.6	60.2	19.9	4.1
65.0	26.3	3.0	65.2	34.8	3.9
70.0	27.8	3.7	70.2	37.6	5.0
80.0	23.8	4.3	80.2	31.6	5.8
85.0	23.9	2.9	85.2	31.8	3.8
90.0	18.5	3.1	90.2	23.5	3.9
100.0	13.9	3.0	100.2	16.8	3.6
105.0	13.2	2.0	105.2	15.9	2.4
110.0	6.5	1.6	110.2	6.1	1.5
120.0	6.1	2.0	120.2	6.1	2.0
130.0	11.0	2.2	130.2	14.0	2.8
140.0	13.6	3.0	140.2	17.8	3.9
150.0	14.4	2.5	150.1	18.7	3.2
160.0	12.9	2.8	160.1	16.1	3.5

LEGENDRE POLYNOMIAL COEFFICIENTS

L	A_L (mb/sr)	Error (%)
0	30.58	19.7
1	34.63	46.0
2	30.34	74.2
3	21.96	111.8
4	32.14	72.0
5	25.98	73.0
6	- 5.22	282.4
7	- 4.82	209.9

TABLE 11 : SCATTERING OF 3.400 ± 0.010 MEV NEUTRONS FROM ^{235}U
LEVEL : 0.103 MeV ($11/2^-$)

PRIOR TO SAMPLE CORRECTIONS			AFTER SAMPLE CORRECTIONS		
θ_{LAB}(deg)	$d\sigma/d\Omega_{LAB}$(mb/sr)	Error (mb/sr)	θ_{CM} (deg)	$d\sigma/d\Omega_{CM}$(mb/sr)	Error (mb/sr)
40.0	14.4	3.2	40.2	19.5	4.3
50.0	10.8	2.1	50.2	14.2	2.8
60.0	8.0	2.3	60.2	10.1	2.9
65.0	7.0	1.3	65.2	8.7	1.7
70.0	6.2	1.6	70.2	7.6	1.9
80.0	6.8	2.0	80.2	8.7	2.6
85.0	9.3	1.6	85.2	12.7	2.2
90.0	8.3	1.9	90.2	11.2	2.6
100.0	6.4	2.0	100.2	8.3	2.6
105.0	5.8	1.2	105.2	7.4	1.6
110.0	4.8	1.4	110.2	5.9	1.8
120.0	3.8	1.5	120.2	4.5	1.8
130.0	3.6	1.3	130.2	4.3	1.5
140.0	3.6	1.5	140.2	4.4	1.8
150.0	3.4	1.2	150.1	4.2	1.4
160.0	3.2	1.4	160.1	3.9	1.7

LEGENDRE POLYNOMIAL COEFFICIENTS

L	A_L (mb/sr)	Error (%)
0	9.96	11.8
1	9.51	29.3
2	5.46	64.2
3	5.43	62.2
4	4.47	59.2

TABLE 12 : *SCATTERING OF 3.400 ± 0.010 MEV NEUTRONS FROM ^{239}Pu*
LEVELS : 0.0 MeV (1/2+)
0.008 MeV (3/2+)

PRIOR TO SAMPLE CORRECTIONS			AFTER SAMPLE CORRECTIONS		
θ_{LAB}(deg)	$d\sigma/d\Omega_{LAB}$(mb/sr)	Error (mb/sr)	θ_{CM} (deg)	$d\sigma/d\Omega_{CM}$(mb/sr)	Error (mb/sr)
20.0	2110.7	154.1	20.1	3123.7	228.1
30.0	1143.1	65.2	30.1	1615.9	92.1
40.0	239.3	22.3	40.2	266.3	24.8
45.0	135.4	10.7	45.2	133.4	10.7
50.0	72.0	6.2	50.2	59.1	5.1
60.0	67.7	10.2	60.2	77.8	11.7
65.0	74.7	6.6	65.2	93.9	8.3
70.0	80.5	7.2	70.2	105.2	9.5
80.0	102.5	10.4	80.2	140.8	14.2
85.0	90.7	7.7	85.2	122.0	10.4
90.0	79.9	7.6	90.2	105.3	10.0
100.0	33.1	3.5	100.2	36.6	3.9
105.0	29.9	3.4	105.2	33.9	3.9
110.0	19.5	2.8	110.2	20.2	2.3
120.0	8.3	1.7	120.2	5.7	1.2
130.0	10.1	2.0	130.2	9.7	2.0
140.0	27.2	3.6	140.2	36.3	4.8
150.0	28.1	3.7	150.1	35.5	4.7
160.0	31.6	3.7	160.1	38.9	4.6

LEGENDRE POLYNOMIAL COEFFICIENTS

L	A_L (mb/sr)	Error (%)
0	339.88	13.6
1	819.50	15.9
2	1108.57	17.7
3	1234.41	19.0
4	1277.86	19.4
5	1069.81	22.0
6	726.71	28.1
7	448.70	36.5
8	260.93	46.5
9	134.78	56.4
10	62.47	67.4

TABLE 13 : SCATTERING OF 3.400 ± 0.010 MEV NEUTRONS FROM ^{239}Pu
LEVELS : 0.057 MeV ($5/2^+$)
0.076 MeV ($7/2^+$)

PRIOR TO SAMPLE CORRECTIONS			AFTER SAMPLE CORRECTIONS		
θ_{LAB}(deg)	$d\sigma/d\Omega_{LAB}$(mb/sr)	Error (mb/sr)	θ_{CM} (deg)	$d\sigma/d\Omega_{CM}$(mb/sr)	Error (mb/sr)
40.0	32.2	5.6	40.2	42.2	7.4
45.0	31.7	3.3	45.2	41.5	4.4
50.0	35.7	4.1	50.2	48.0	5.5
60.0	27.3	5.2	60.2	35.3	6.8
65.0	25.7	2.8	65.2	33.0	3.6
70.0	26.1	3.5	70.2	33.9	4.5
80.0	25.0	5.1	80.2	32.6	6.6
85.0	27.8	3.0	85.2	37.2	4.0
90.0	23.4	3.4	90.2	30.5	4.4
100.0	19.0	2.6	100.2	24.0	3.3
105.0	12.8	1.9	105.2	14.7	2.2
110.0	14.3	2.5	110.2	17.3	3.0
120.0	9.1	1.8	120.2	9.8	1.9
130.0	16.4	2.8	130.2	21.2	3.6
140.0	17.7	2.5	140.2	22.8	3.3
150.0	20.5	3.2	150.1	26.4	4.1

LEGENDRE POLYNOMIAL COEFFICIENTS

L	A_L (mb/sr)	Error (%)
0	30.25	10.2
1	17.66	40.1
2	10.53	94.1
3	- 7.39	146.2
4	7.48	144.4
5	3.81	250.0
6	- 11.36	81.2
7	- 3.65	269.7

TABLE 14 : SCATTERING OF 3.400 ± 0.010 MEV NEUTRONS FROM ^{239}Pu
LEVELS : 0.164 MeV ($9/2^+$)
0.193 MeV ($11/2^+$)

PRIOR TO SAMPLE CORRECTIONS			AFTER SAMPLE CORRECTIONS		
θ_{LAB}(deg)	$d\sigma/d\Omega_{LAB}$(mb/sr)	Error (mb/sr)	θ_{CM} (deg)	$d\sigma/d\Omega_{CM}$(mb/sr)	Error (mb/sr)
65.0	6.6	1.4	65.2	8.7	1.9
70.0	4.3	1.3	70.2	5.1	1.5
85.0	8.2	1.5	85.2	11.2	2.0
90.0	6.9	1.7	90.2	9.1	2.2
105.0	5.0	1.1	105.2	6.0	1.3
110.0	8.3	1.8	110.2	11.1	2.4
130.0	8.3	1.9	130.2	11.1	2.5
140.0	6.0	1.5	140.2	7.6	1.9
160.0	4.0	1.3	160.1	4.7	1.5

LEGENDRE POLYNOMIAL COEFFICIENTS

L	A_L (mb/sr)	Error (%)
0	8.23	29.8
1	1.61	306.6
2	0.86	668.9
3	3.25	144.9
4	- 0.85	585.1

TABLE 15

Comparison of evaluated and experimental angle-integrated neutron inelastic scattering cross sections of ^{232}Th, ^{238}U, ^{235}U and ^{239}Pu. Data are given in mb.

NUCLEUS	^{232}Th		^{238}U		^{235}U			^{239}Pu		
State	2^+ (50 keV)	4^+ (163 keV)	2^+ (45 keV)	4^+ (148 keV)	$9/2^-$ (46 keV) $+5/2^+$ (52 keV)	$7/2^+$ (84 keV)	$11/2^-$ (103 keV)	$3/2^+$ (8 keV)	$5/2^+$ (57 keV) $+7/2^+$ (76 keV)	$9/2^+$ (164 keV) $+11/2^+$ (193 keV)
ENDF/BIV	34	51	165	6	52	12	12	3.2	3.2	4.2
ENDL 76			418	121				0	55	4
This work	562 ± 73	183 ± 12	576 ± 71	147 ± 10	384 ± 75	0	125 ± 15	-	380 ± 39	103 ± 31

TABLE 16

Potential parameters used in this study. Potential depths and incident neutron energy E are given in MeV. Radii and diffusivenesses are given in fm.

	V_R : REAL POTENTIAL	W_D : SURFACE IMAGINARY POTENTIAL	V_{SO} : SPIN-ORBIT POTENTIAL
Nucleus \ Geometric parameters	$R_R^o = 1{,}26$ $a_R = 0{,}63$	$R_D^o = 1{,}26$ $a_D = 0{,}52$	$R_{SO}^o = 1{,}12$ $a_{SO} = 0{,}47$
^{208}Pb	46,4(± 0,2) - 0,3 E	2,3 (± 0,3) + 0,45 E	8,4 ± 0,3
^{232}Th	46,4(± 0,2) - 0,3 E	3,6 (± 0,2) + 0,4 E	6,2 ± 0,3
^{235}U	46,4(± 0,2) - 0,3 E	3,3 (± 0,2) + 0,4 E	6,2 ± 0,3
^{238}U	46,2(± 0,2) - 0,3 E	3,6 (± 0,2) + 0,4 E	6,2 ± 0,3
^{239}Pu	46,2(± 0,2) - 0,3 E	3,6 (± 0,2) + 0,4 E	6,2 ± 0,3

TABLE 17

Values of quadrupole (β_2) and hexadecapole (β_4) deformation parameters.

NUCLEUS	^{232}Th	^{238}U	^{235}U	^{239}Pu
β_2	0.190	0.198	0.220	0.220
β_4	0.071	0.057	0.080	0.070

FIGURE CAPTIONS

Fig.1 Low-lying level schemes of ^{208}Pb, ^{232}Th, ^{235}U, ^{238}U and ^{239}Pu. Excitation energies are given in MeV.

Fig.2 Time-of-flight spectrum of 3.4 MeV neutrons scattered at 105 deg. by ^{238}U. The flight path is 10 m. The experimental resolution is $\sim$ 28 keV for the elastic peak. The low-lying states of ^{238}U are marked by arrows.

Fig.3 Time-of-flight spectrum of 3.4 MeV neutrons scattered at 105 deg by ^{235}U. The flight path is 10 m. In this figure, the low-lying states of ^{235}U are marked by arrows.

Fig.4 Time-of-flight spectrum for ^{239}Pu at 3.4 MeV incident neutron energy for a scattering angle of 105 deg. The flight path is 10 m. The low-lying states of ^{239}Pu are marked by arrows.

Fig.5 Differential elastic neutron scattering cross sections at 3.4 MeV incident energy for ^{208}Pb. The upper solid curve is the sum of the compound nucleus (CN) plus direct interaction (DI) theoretical calculations. Separated contributions are shown as dashed (DI) and dotted (CN) curves.

Fig.6 Neutron scattering cross sections at 3.4 MeV for elastic (0^+), first excited (2^+, 50 keV) and second excited (4^+, 162 keV) states in ^{232}Th. The solid curves are results of theoretical calculations as described in the text.

Fig.7. Neutron scattering cross sections at 3.4 MeV for elastic (0^+), first excited (2^+, 45 keV) and second excited (4^+, 148 keV) states in ^{238}U. The solid curves are results of theoretical calculations as described in the text.

Fig.8 Neutron scattering cross sections of ^{235}U at 3.4 MeV for the two groups of levels : [$7/2^-$ (g.s), $1/2^+$ (75 eV), $3/2^+$ (13 keV)], [$9/2^-$ (46 keV), $5/2^+$ (52 keV)], and for the $11/2^-$ (103 keV) state. The solid curves are results of theoretical calculations discussed in the text.

Fig.9 Neutron scattering cross sections of ^{239}Pu at 3.4 MeV for the three groups of levels : [$1/2^+$ (g.s), $3/2^+$ (8 keV)] [$5/2^+$ (57 keV), $7/2^+$ (76 keV)] and [$9/2^+$ (164 keV), $11/2^+$ (193 keV)]. The solid curves are results of coupled-channel calculations taking into account explicitly the coupling of the $1/2^+$, $3/2^+$, $5/2^+$, $7/2^+$, $9/2^+$ states. The dashed curves are results of calculations based on the adiabatic approximation.

Fig.10 Differential elastic scattering cross sections at 3.4 MeV incident neutron energy for ^{208}Pb, ^{232}Th and ^{238}U and cross sections for the groups of levels : ($7/2^-$, $1/2^+$, $3/2^+$) for ^{235}U and ($1/2^+$, $3/2^+$) for ^{239}Pu. The solid lines are the results of coupled-channel calculations as described in the text. The dotted and dashed curves are the angular distributions deduced from the ENDF/B IV and ENDL 76 files, respectively.

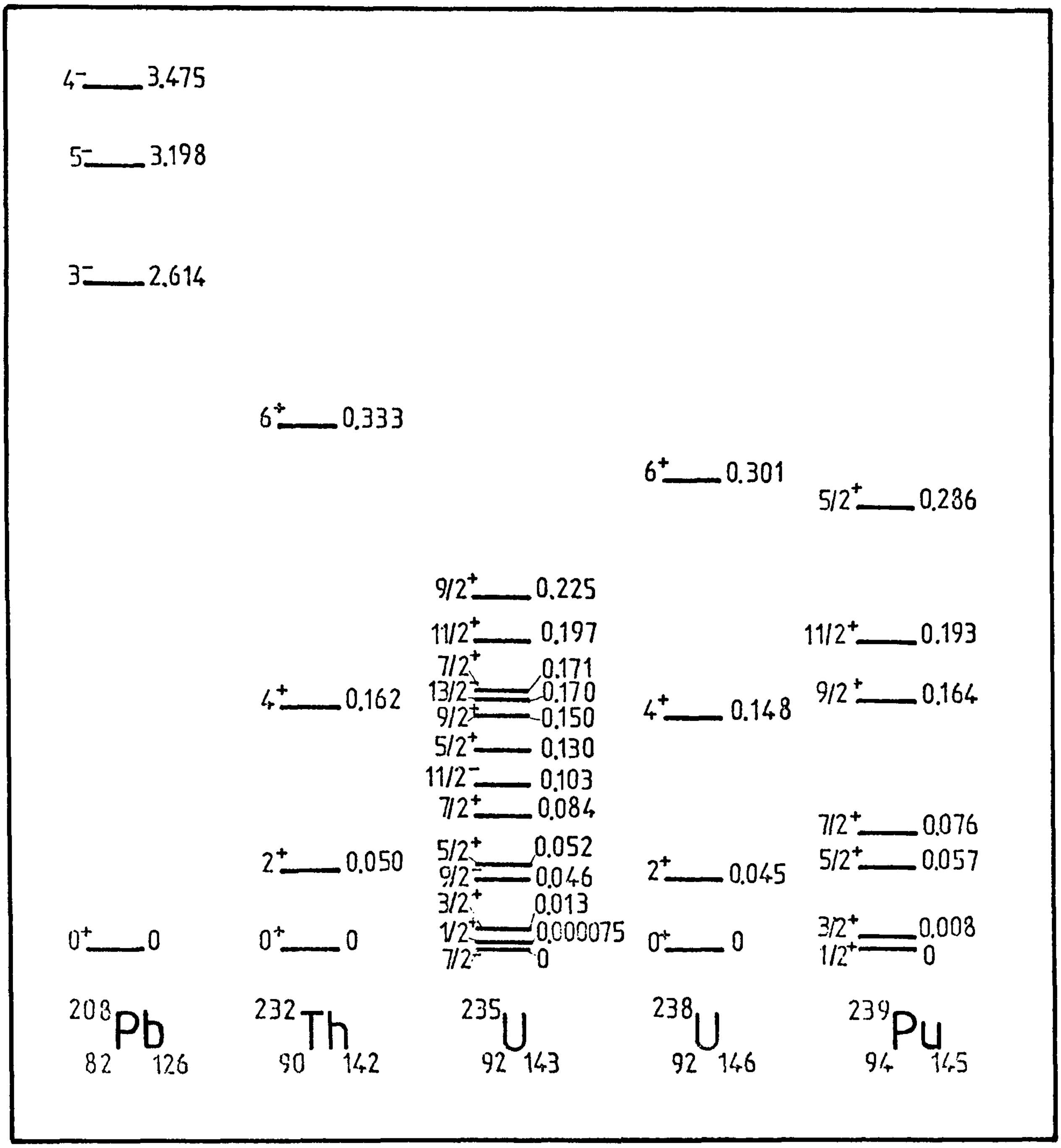

4⁻ 3.475
5⁻ 3.198
3⁻ 2.614
0⁺ 0
208 Pb 82 126
6⁺ 0.333
4⁺ 0.162
2⁺ 0.050
0⁺ 0
232 Th 90 142
9/2⁺ 0.225
11/2⁺ 0.197
7/2⁺ 0.171
13/2⁻ 0.170
9/2⁺ 0.150
5/2⁺ 0.130
11/2⁻ 0.103
7/2⁺ 0.084
5/2⁺ 0.052
9/2⁻ 0.046
3/2⁺ 0.013
1/2⁺ 0.000075
7/2⁻ 0
235 U 92 143
6⁺ 0.301
4⁺ 0.148
2⁺ 0.045
0⁺ 0
238 U 92 146
5/2⁺ 0.286
11/2⁺ 0.193
9/2⁺ 0.164
7/2⁺ 0.076
5/2⁺ 0.057
3/2⁺ 0.008
1/2⁺ 0
239 Pu 94 145

Fig. 1

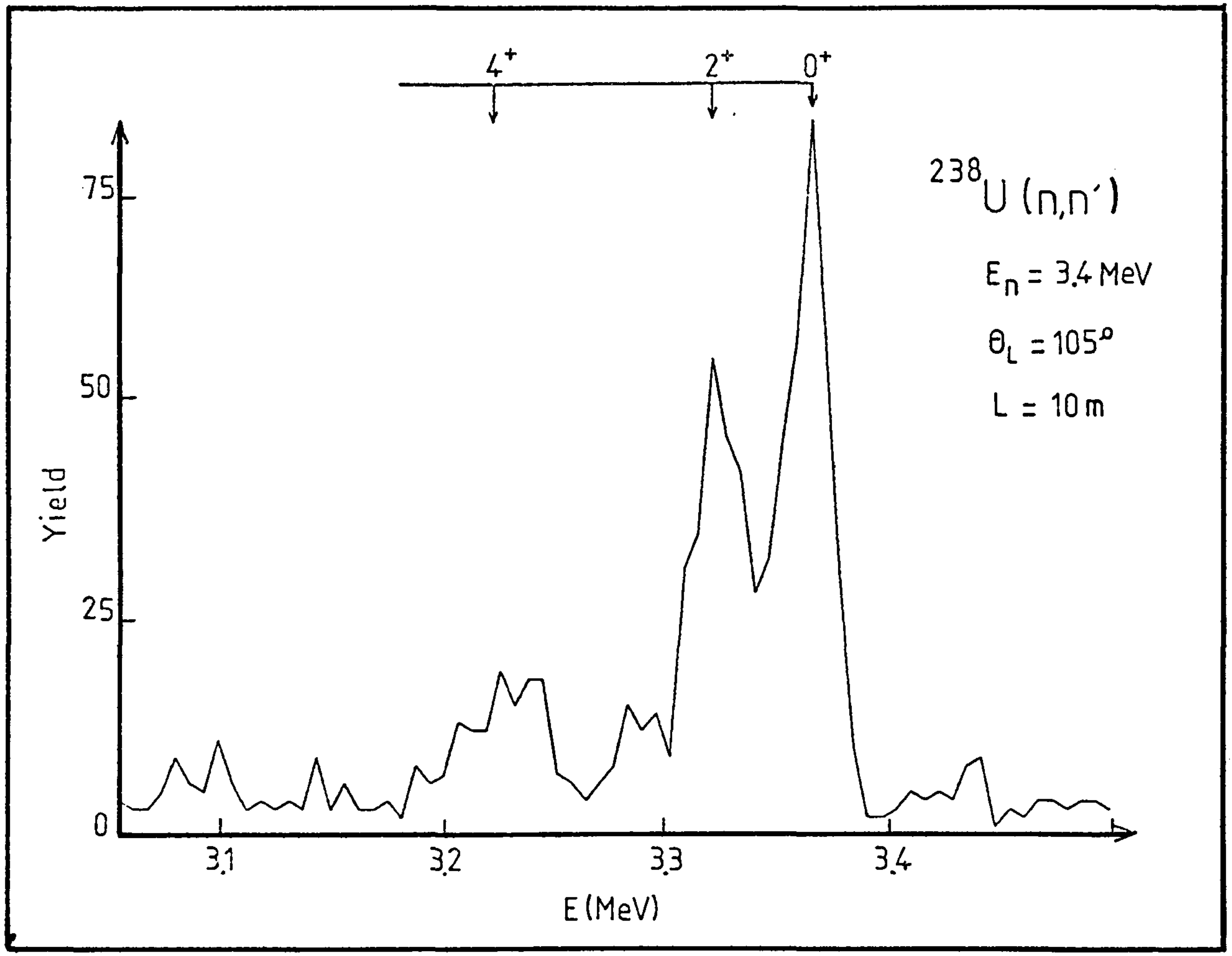

Fig. 2

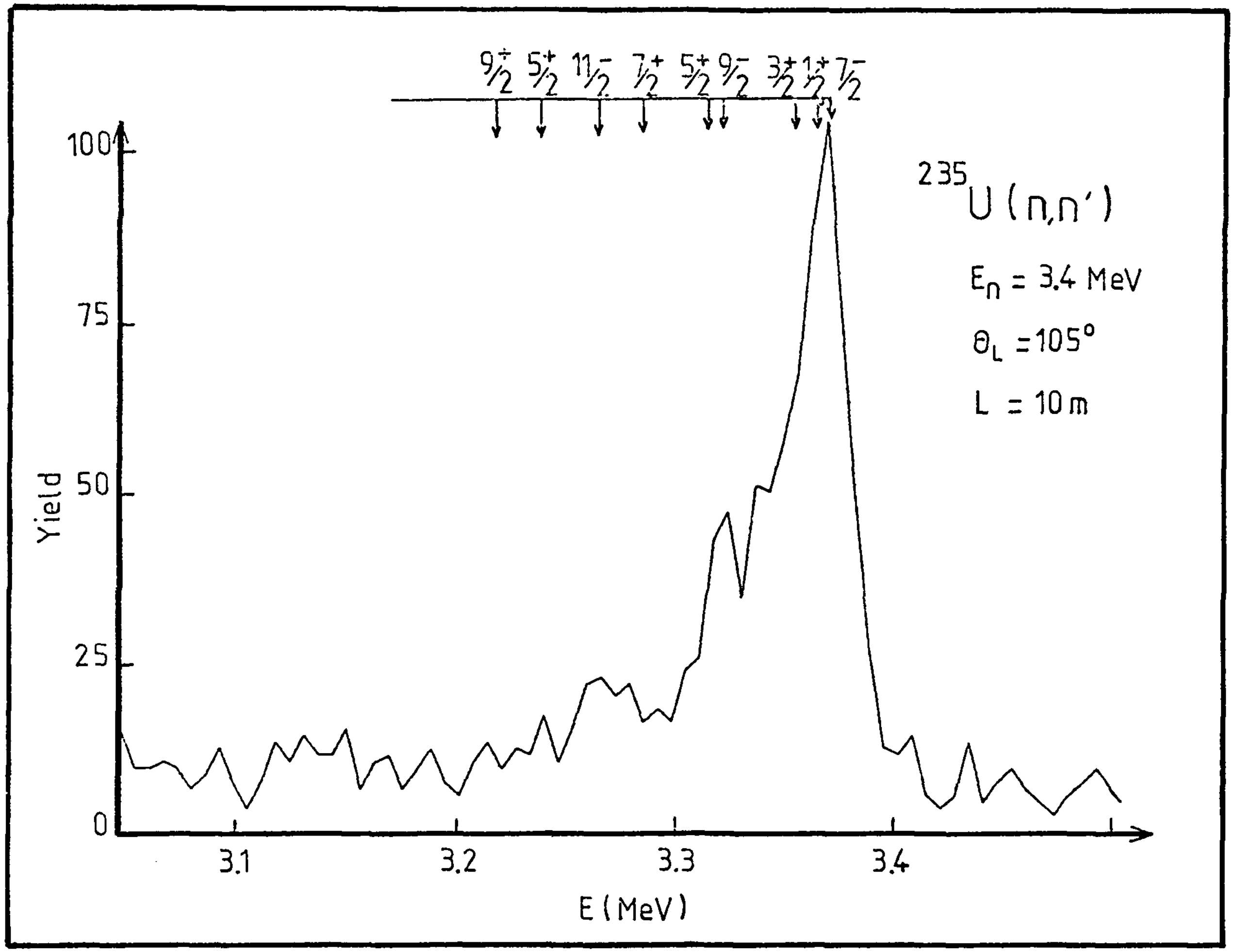

9/2+ 5/2+ 11/2- 7/2+ 5/2+ 9/2- 3/2+ 1/2+ 7/2-
^{235}U (n,n')
E_n = 3.4 MeV
θ_L = 105°
L = 10 m
Yield
100
75
50
25
0
3.1
3.2
3.3
3.4
E (MeV)

Fig. 3

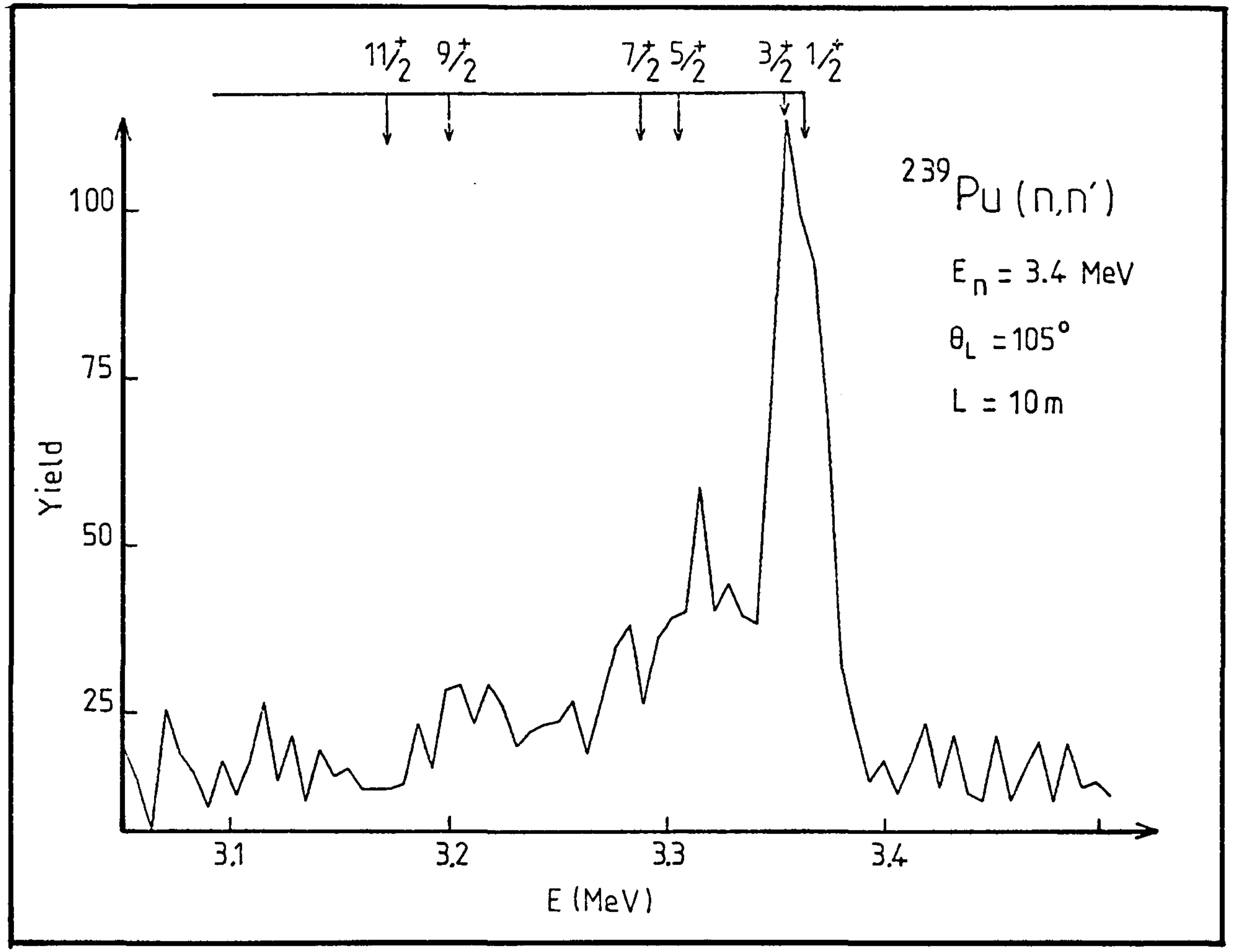

11/2+ 9/2+ 7/2+ 5/2+ 3/2+ 1/2+
239Pu (n,n')
En = 3.4 MeV
θL = 105°
L = 10 m
Yield
100
75
50
25
3.1
3.2
3.3
3.4
E (MeV)

Fig. 4

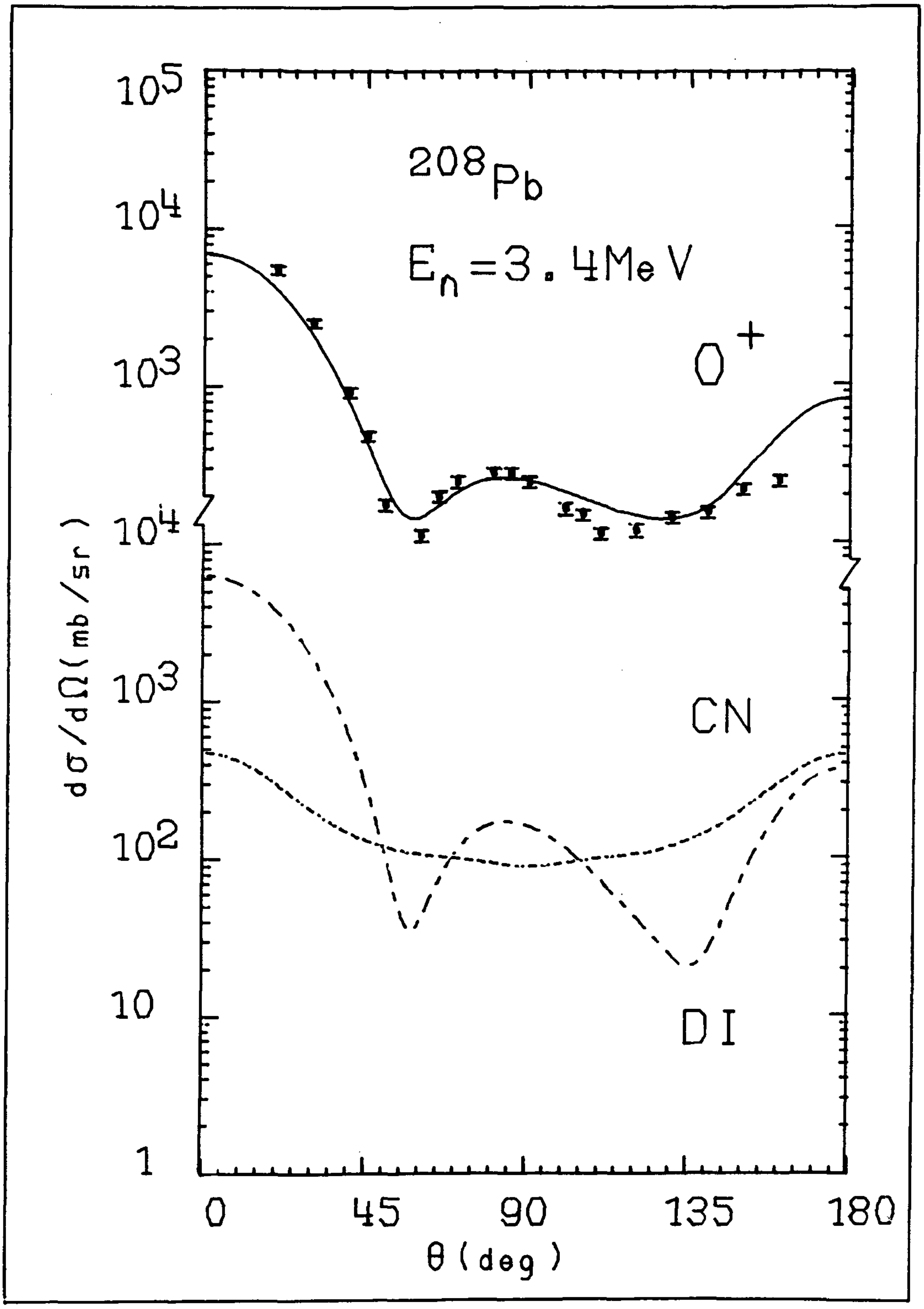
10^5
10^4
10^3
10^4
10^3
10^2
10
1
^{208}Pb
$E_n = 3.4$ MeV
0^+
CN
DI
$d\sigma/d\Omega$ (mb/sr)
0
45
90
135
180
θ (deg)

Fig.5

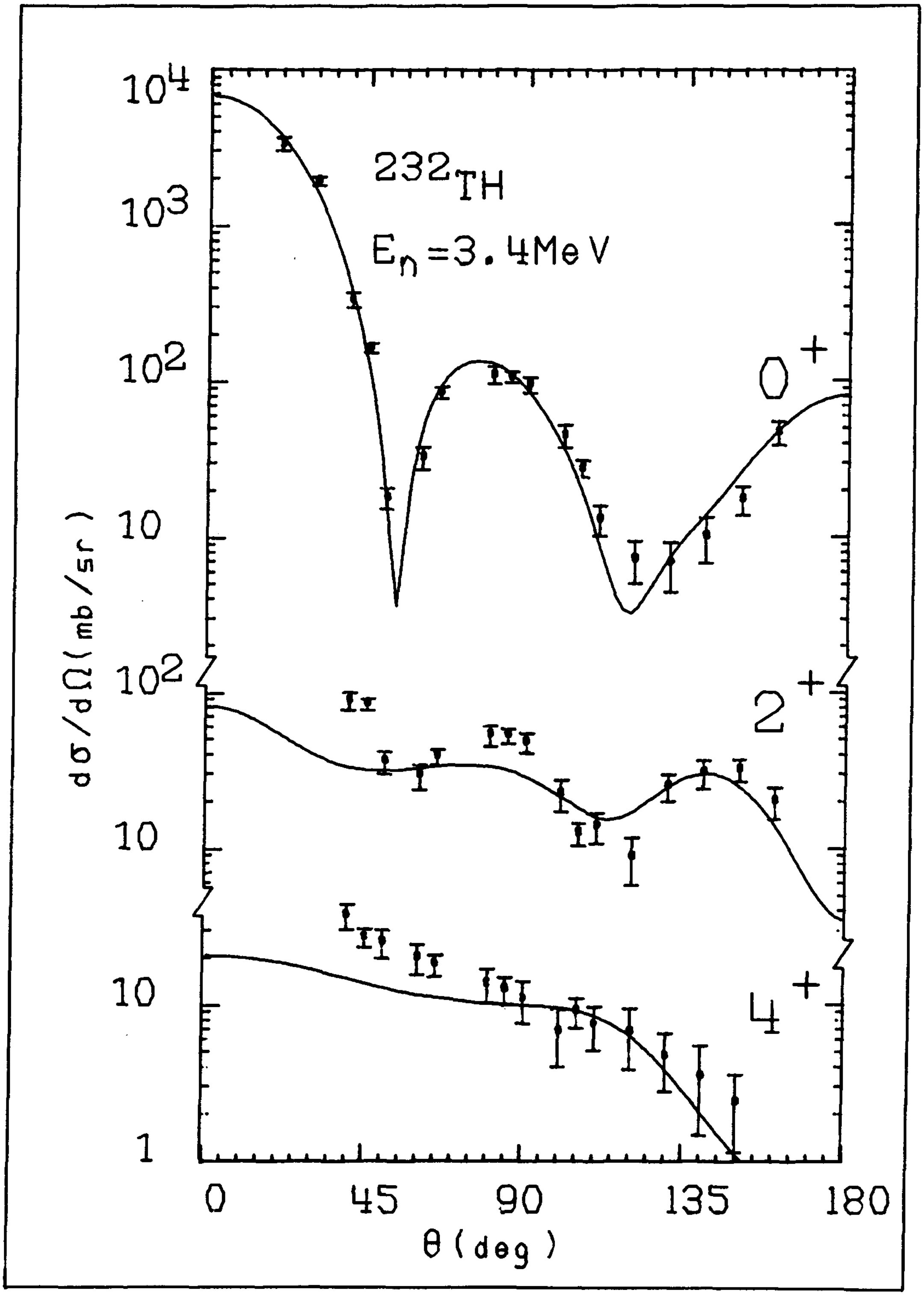

10^4
10^3
10^2
10
10^2
10
10
1
^{232}TH
E_n=3.4MeV
0^+
2^+
4^+
$d\sigma/d\Omega$(mb/sr)
0
45
90
135
180
θ(deg)

Fig. 6

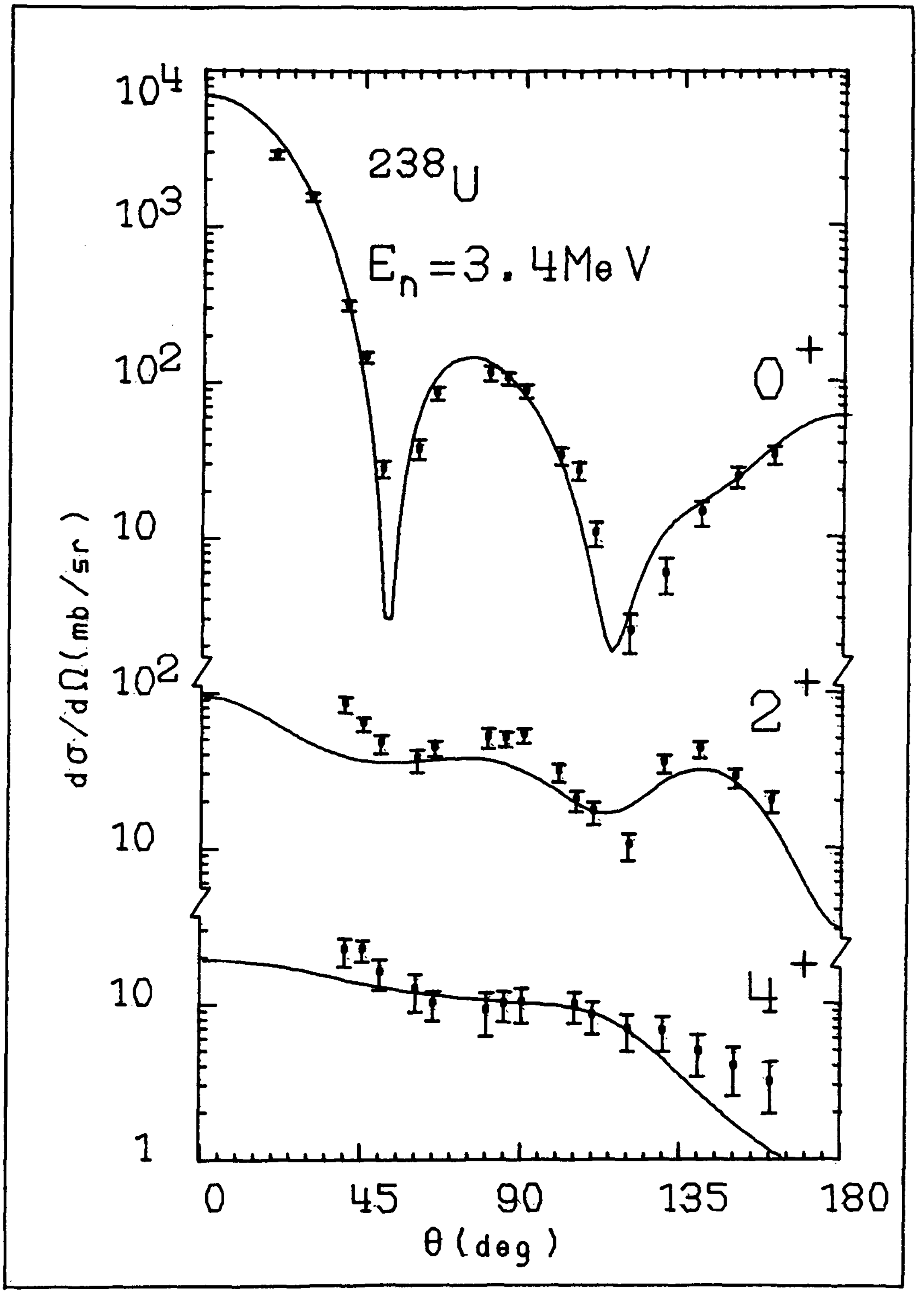
10^4
10^3
10^2
10
10^2
10
10
1
^{238}U
$E_n=3.4MeV$
0^+
2^+
4^+
$d\sigma/d\Omega$ (mb/sr)
0
45
90
135
180
θ (deg)

Fig. 7

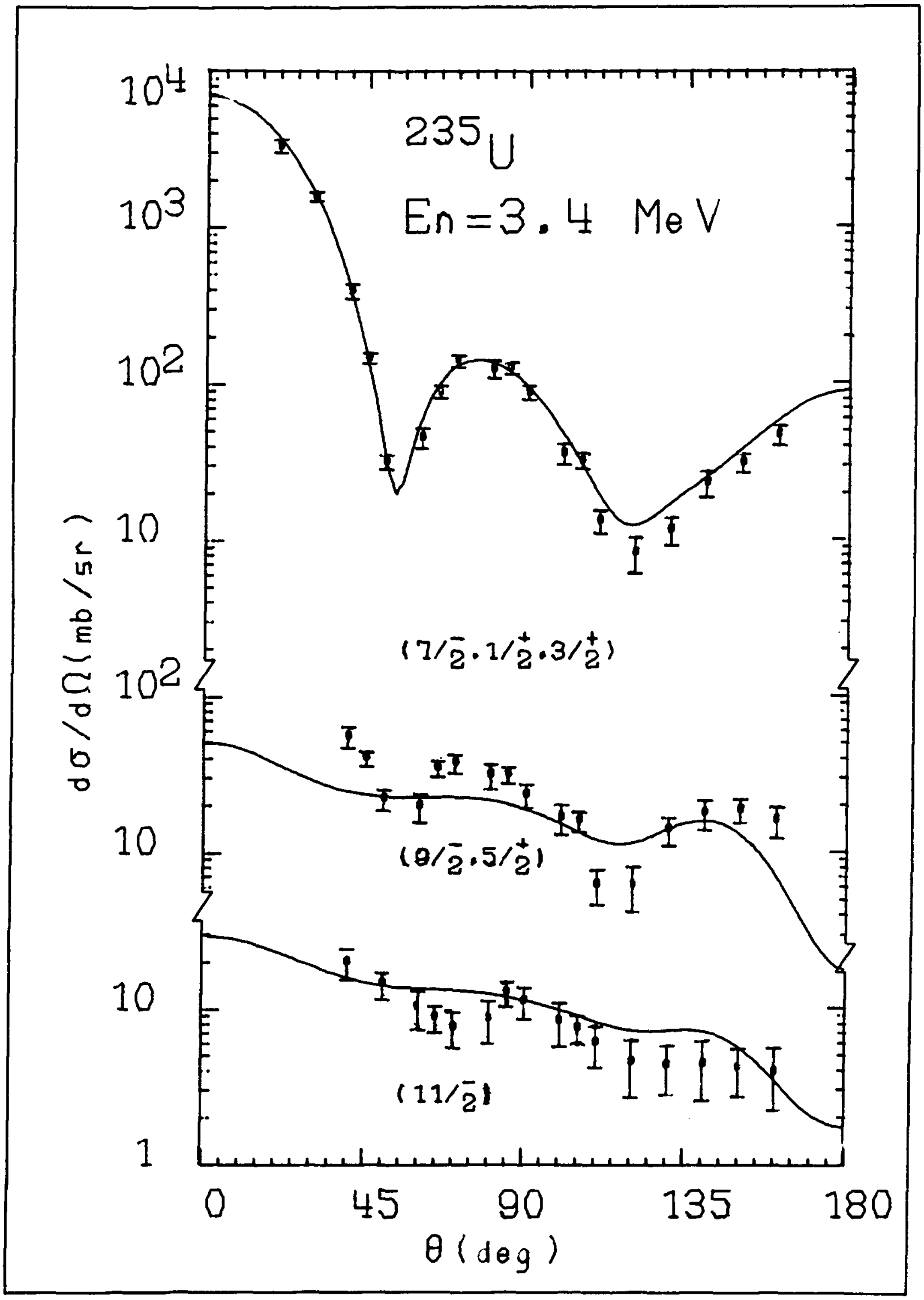
10^4
10^3
10^2
10
10^2
10
10
1
^{235}U
En = 3.4 MeV
$(7/2^-, 1/2^+, 3/2^+)$
$(9/2^-, 5/2^+)$
$(11/2^-)$
dσ/dΩ (mb/sr)
0
45
90
135
180
θ (deg)

Fig. 8

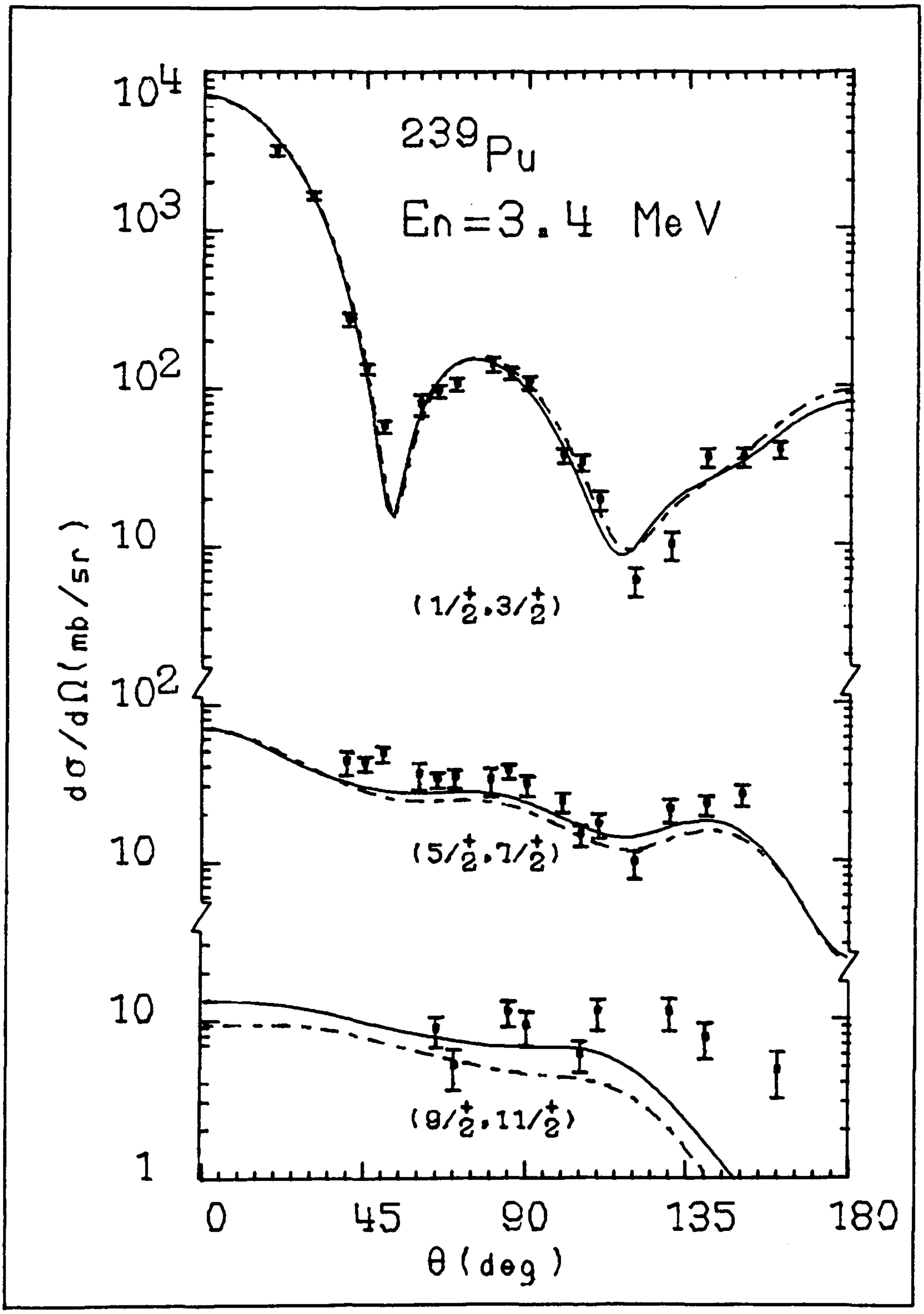
10^4
10^3
10^2
10
10^2
10
10
1
^{239}Pu
En=3.4 MeV
$(1/2^+, 3/2^+)$
$(5/2^+, 7/2^+)$
$(9/2^+, 11/2^+)$
dσ/dΩ(mb/sr)
0
45
90
135
180
θ(deg)

Fig. 9

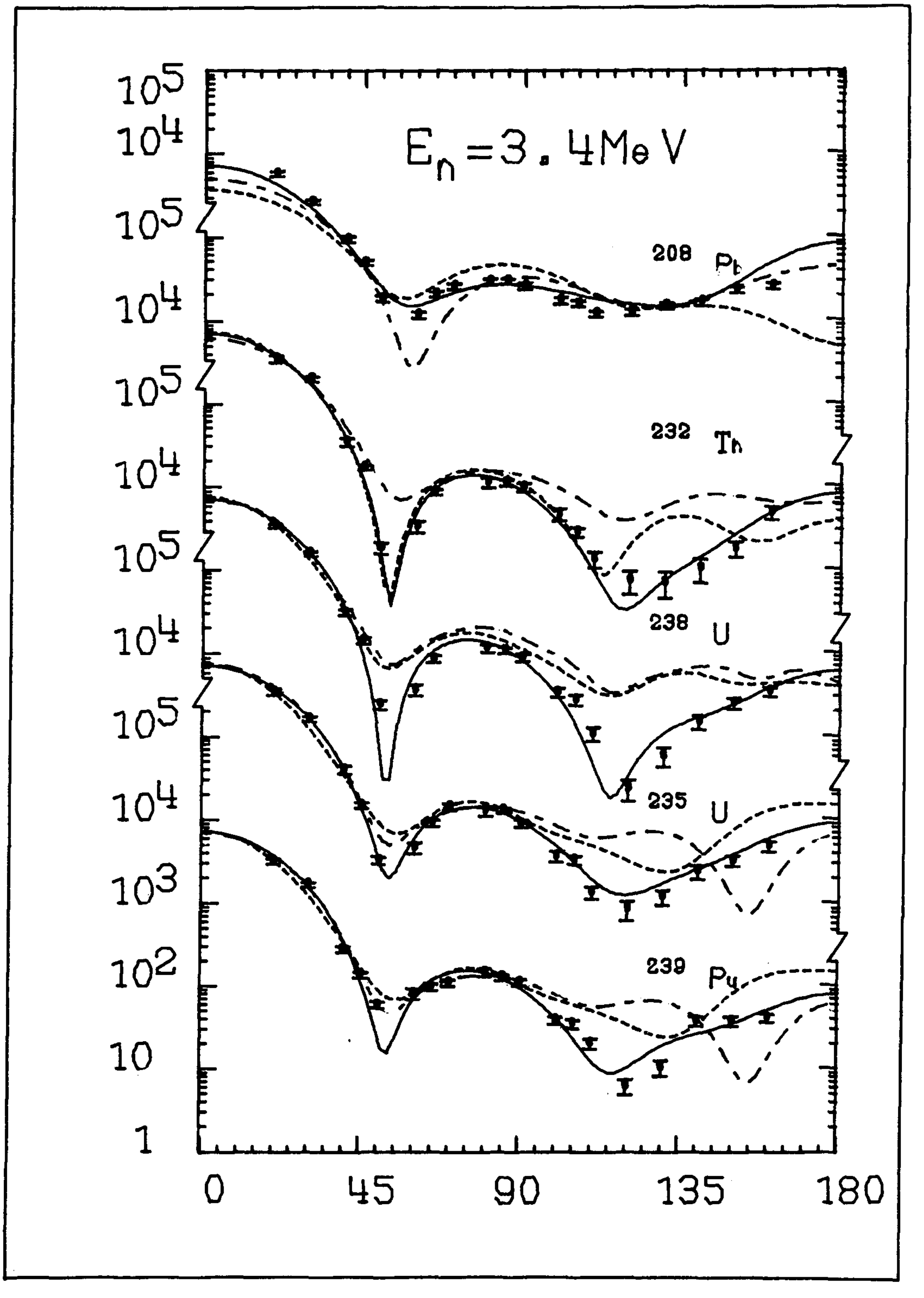

$E_n = 3.4MeV$
208 Pb
232 Th
238 U
235 U
239 Pu
10^5
10^4
10^3
10^2
10
1
0
45
90
135
180

Fig. 10